Lasers in Manufacturing Conference 2025

Laser melt injection of spherical fused tungsten carbide and niobium carbide on aluminium bronze substrates for enhanced cavitation erosion resistance

Minkeshkumar Ramoliya[a, *], Annika Bohlen[a], Thomas Seefeld[a,b]

[a]*BIAS – Bremer Institut fuer angewandte Strahltechnik GmbH, Klagenfurter Strasse 5, 28359 Bremen, Germany*
[b]*MAPEX Center for Materials and Processes – Universtiy of Bremen, Bibliothek Strasse 1, 28359 Bremen, Germany*

Abstract

Cavitation erosion (CE) is detrimental to a number of engineering components, including ship propellers and pump impellers. Due to deformation and mass loss, CE significantly impairs the serviceability of these components and results in tremendous economic loss. Therefore, the demand for a reduction in material damage due to CE is imperative. Material damage can be minimised by using protective layers tailored to resist CE. In this work, laser melt injection (LMI) was performed to improve the cavitation erosion resistance. A metal matrix composite (MMC) is formed on the aluminium-bronze substrates by injecting spherical fused tungsten carbide (SFTC), or niobium carbide (NbC). The impact of different particle sizes on the CE behavior of the reinforced surface layer was investigated. CE tests of produced layers and untreated aluminium bronze are carried out as per ASTM G32-16 standard and the results are compared. The dependency of coating initial surface roughness, microhardness, and fracture toughness of particles on the cavitation erosion is discussed. It was determined that the small particle-reinforced NbC coating was the most effective in shielding substrates from cavitation damage.

Keywords: laser melt injection, metal matrix composite, cavitation erosion, aluminium bronze, spherical fused tungsten carbide, niobium carbide ;

1. Introduction

Aluminium bronze refers to alloys made of copper and aluminium. It has a reputation for having high strength and great resistance to impingement, erosion, biofouling, and corrosion. Therefore, marine components, including valves, pumps, and ship propellers are often made of aluminium bronze alloy (Song et al. 2017). Typically, either nickel-aluminium bronze (NAB) or manganese-nickel-aluminium bronze is used to make ship propellers. In the current study, we aim to address the cavitation erosion (CE) problem of NAB alloy (Tang et al. 2006).

CE is a common problem in marine parts such as propellers exposed to high-speed fluid flow conditions. The term "cavitation" can be explained by Bernoulli's equation, which refers to high flow velocities leading to a decrease in the local pressure resulting in bubble formation when the pressure falls below vapour pressure. The bubble will collapse under high pressure, producing shock waves or microjets that will pierce the solid surface as the bubble implodes close to it. Such recurring events will lead to wear and tears and the loss of surface material. This phenomenon is called cavitation erosion. When cavitation is strong enough, it can eventually destroy a component by creating a porous matrix (Kwok et al. 2016; Tang et al. 2004). The propeller, among other parts of the ship's appendages, is particularly prone to cavitation. The propeller's leading edge, blade tip, and hub are most prone to cavitation (Peters et al. 2018). In Fig. 1 cavitation damage can be seen on the blade of the ship's propeller. Therefore, increasing the wear and corrosion resistance and perpetuating the lifespan of NAB alloy components for maritime applications is essential.

There are three different approaches to diminish cavitation damage. One is to design optimisation of hydraulic components, the second is to change the environmental conditions of the fluids, and another is to apply a protective layer

* Corresponding author. Tel.: +49 421 218 58068 fax: +49 421 218 58063.
E-mail address: ramoliya@bias.de.

against CE. Considering that design optimisation and changing environmental conditions are challenging, the third approach is the more appropriate (García-García et al. 2006; Zheng et al. 2008).

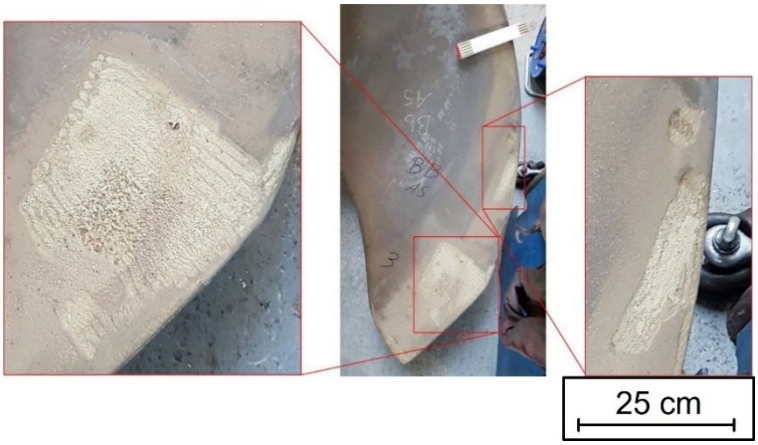

Fig. 1. Cavitation damage to the blade of the ship's propeller (Quelle: LaserCladdingGermany GmbH).

In recent years, laser melt injection (LMI)-deposited metal matrix composite (MMC) layers with diversified volume percentages of ceramic particles have attracted greater scrutiny for their potential to enhance surface qualities (V. Ocelík et al. 2003; Freiße et al. 2019). Fig. 2 shows the principle of the laser melt injection. During the LMI process, a laser beam is used to melt the metal substrate's surface layer while concurrently adding powder additive (in our case a carbide powder) to the melt pool. An MMC layer forms due to the melt pool's rapid solidification, which captures particles. Carbides acquire distinctive properties like high hardness, excellent abrasion resistance, corrosion resistance, and good compatibility with metal matrix. Therefore, carbides make the most sense as metal matrix reinforcements (Li et al. 2021). Spherical fused tungsten carbide (SFTC) is mainly used as a reinforcement particle in the NAB matrix, while less research has been published on the LMI of niobium carbide (NbC). NbC has high hardness (2400 HV), high melting temperature (3600 ºC), large thermal expansion coefficient, and high-temperature deformation resistance. Furthermore, NbC also has a much lower density (7.79 g/cm^3) and stronger antioxidant capacity than SFTC (Zhao et al. 2016). Gualtieri et al. (Gualtieri und Bandyopadhyay 2017) reported an NbC composite coating prepared on SS304 by laser overlay welding to improve the wear rate. Their study showed a decrease in the wear rate of matrix SS304 by > 75%. Producing SFTC and NbC-reinforced MMC using NAB alloy is encouraging.

In addition to the composition of the metallic matrix and the particle, the form, size, distribution, and percentage of the particles in the MMC all have a significant impact on its qualities (Freiße et al. 2019).

Kolbe et al. (Kolbe G 2005) have injected various borides like TiB_2, ZrB_2, and CrB_2 into a horn made of a TiAl6V4 matrix. The powder particle size has been shown to affect cavitation wear. It has been reported that fine powders produce a uniform and fined-grained microstructure compared to larger particles. The layer produced with fine powders increases the microhardness by 75% and cavitation wears up to 75%.

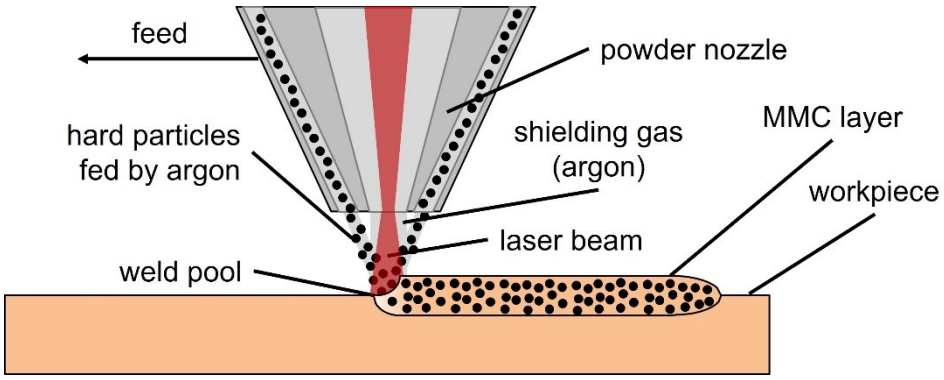

Fig. 2. Schematic of laser melt injection process.

In the present study, MMC layers were fabricated on an NAB alloy by laser melt injection using SFTC, and NbC powders with different particle sizes as reinforcement and metal matrix respectively. To examine how particle size affects CE resistance, three different grain fractions (45 µm - 63 µm, 63 µm - 90 µm, and 90 µm - 106 µm) are categorized and made accessible. In this paper, the cavitation erosion performances of SFTC and NbC composite coatings were evaluated according to ASTM G32-16. This research aimed to prepare CE-resistant MMC coating on NAB surfaces for marine applications.

2. Experimental procedure

2.1. Preparation of MMC layers

In this work, NAB (nickel aluminium bronze) alloy was used as the substrate material. The substrate specimens were the size of 50 mm × 40 mm × 20 mm, which were prepared by milling. Two types of hard particles were chosen for the generation of MMCs: SFTC particles (Oerlikon MetcoClad 52001) with particle size range between 45 µm and 106 µm and NbC powder (GTV Verschleißschutz GmbH) with a particle size range of 10 µm to 63 µm. The particle morphology of SFTC and NbC was

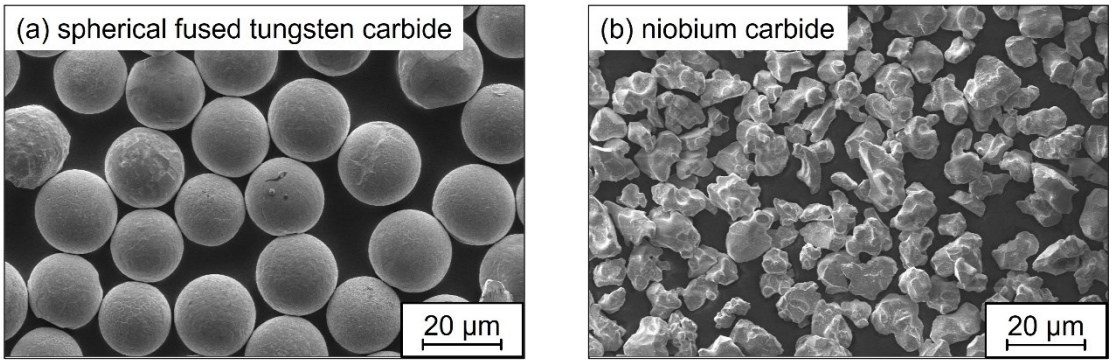

Fig. 3. SEM micrograph showing the morphology of spherical fused tungsten carbide and niobium carbide.

examined by SEM analysis. The SFTC particles exhibited a spherical morphology, while NbC particles showed crushed morphology (as shown in Fig. 3). Table 1 provides a summary of the alloying elements, density, and hardness of all powders and NAB alloys.

A Trumpf TruDisk 12002-disc laser, which has a maximum output power of 12 KW and emits radiation with a wavelength of 1030 nm, is used to execute the laser melt injection (LMI) process. It was directed to a processing optic (Trumpf BEO D70) using an optical cable with a core diameter of 200 µm, a collimation length of 200 mm, and a focal length of 250 mm. Throughout the experiment, the laser spot diameter has been set at 3 mm, and the defocusing distance is 21 mm. A 3-axis CNC was used to direct the processing optic. The processing head was tilted by 8° from the vertical in the direction of travel to prevent any damage caused by back reflection. The six-jet powder nozzle (GTV PN6625) was used with a working distance of 25 mm. An Oerlikon Metco Twin 150 rotating disc powder feeder was used to carry the carbide particles to the powder nozzles. Argon was employed as a carrier gas and shielding gas, with flow rates of 4.5 l/min and 7 l/min, respectively. To cut the prepared MMC specimens, wire EDM was used, and the cross sections were then polished and ground.

Table 1. Chemical composition, density, and hardness of the NAB, SFTC, and NbC (Oerlikon Metco; GTV Verschleißschutz GmbH).

Material	Chemical composition in wt.%									Density (g/cm^3)	Hardness (HV)
	Cu	Al	Ni	Fe	Mn	W	Nb	C	Other		
NAB	Bal.	10	5	4	1	-	-	-	-	7.6	217
SFTC	-	-	-	-	-	Bal.	-	3.8	0.7	15.6	2600
NbC	-	-	-	-	-	-	Bal.	11.25	0.36	7.8	2400

2.2. Cavitation erosion test

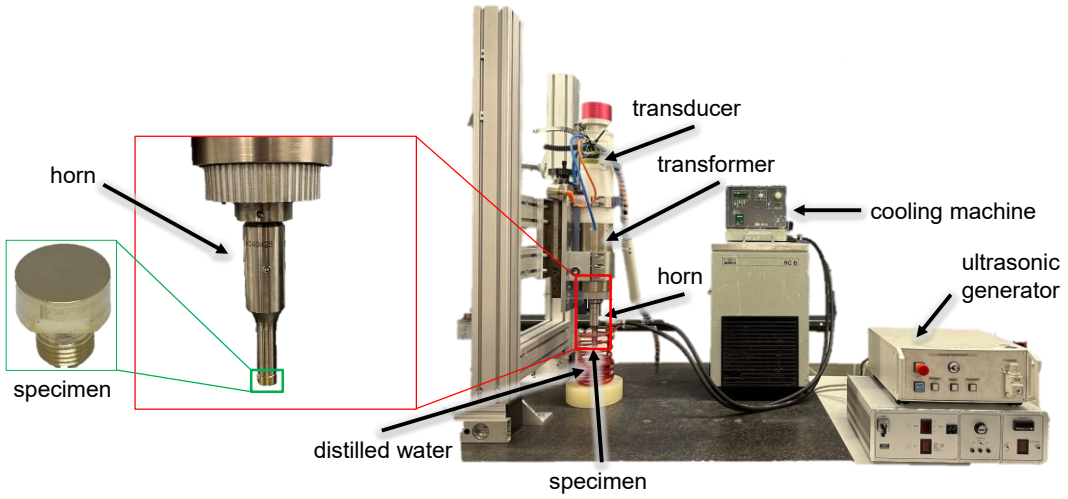

Fig. 4. Schematic of vibratory cavitation erosion apparatus according to ASTM G32-16.

After LMI, three types of cavitation samples were made from the rectangular substrate by cutting out the round samples with 16 mm diameter and 18 mm height using EDM, and then threads were turned, which are listed in Table 2. All the samples were polished by diamond polishing and had a roughness of Sa < 0,2 µm. Additionally, two unpolished NbC particle-reinforced samples with different particle sizes were produced to comprehend the impact of surface roughness on cavitation erosion. According to the ASTM G32-16 standard (Standard test method for cavitation erosion using vibratory apparatus, G32-16, Annual Book of ASTM 2016), CE tests were performed using a vibratory apparatus. Fig. 4 shows the schematic of the vibratory CE apparatus. An ultrasonic transducer is used, which is attached to the horn or transformer. The specimen is mounted by threading through the horn's tip. The specimen is submerged in deionised water and vibrated at an amplitude of 50 µm and a frequency of 20 kHz. The test liquid was kept at 25°C. Every sample was put through 140 hours of CE testing, done in cycles of 20 hours. The sample's mass was compared to its starting mass after each cycle to determine the mass loss. The mass was weighed with a precision of 1 mg. After a given duration of time, the mean depth erosion (MDE), mean depth erosion rate (MDER), and normalised cavitation erosion resistance were calculated using Eqs. 1, 2, and 3 based on mass loss (Δm). After each cycle, images of the samples were taken using the confocal laser microscope (Keyence VKX-3000).

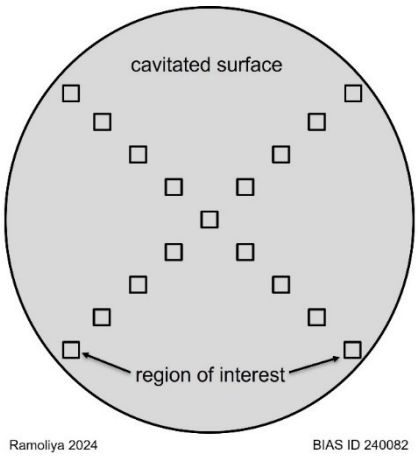

Fig. 5. Regions of interest for measurement of particle volume loss vs surface volume loss for SFTC reinforced sample for density measurements of MMC.

$$\text{Mean depth of erosion}: MDE\ (\mu m) = \Delta m\ /\rho \times A \quad (1)$$

$$\text{Mean depth of erosion rate}: MDER\ (\mu m/hr) = MDE/t \quad (2)$$

$$\text{Normalised cavitation erosion resistance}: Re\ (hr/\mu m) = (MDER) - 1 \quad (3)$$

where ρ is the material density, A is the sample's surface area, Δm is the mass loss of the samples, and t is the overall test duration.

One key figure for the quantification of CE is the volume loss. The volume loss is determined by dividing mass loss by the density of the sample. The density of the eroded areas was determined by estimating the percentage of the eroded particles and matrix since MMCs consist of two materials with different densities and each one of them can have a different erosion rate. To calculate so, images using a confocal laser microscope with high magnification of cavitation samples after 140 hours of testing were taken at several regions (as shown in Fig. 5). The average percentage of erosion of particles and surfaces was calculated for each image taken at the ROIs, resulting in the average percentage of volume loss and density. This approach was used to assess the density of SFTC-reinforced samples. Whereas the density of NbC and NAB is approximately similar. Hence for NbC-reinforced MMC samples, the NAB's density has been considered.

Table 2. Different types of samples produced for the cavitation erosion test.

Samples	Particle size	Description
NAB alloy		Serves as a reference sample
NbC reinforced MMC sample	10 µm - 45 µm	NAB + NbC (10 µm - 45 µm)
	45 µm - 63 µm	NAB + NbC (45 µm - 63 µm)
SFTC reinforced MMC sample	45 µm - 63 µm	NAB + SFTC (45 µm - 63µm)
	63 µm - 90 µm	NAB + SFTC (63 µm - 90µm)
	90 µm - 106 µm	NAB + SFTC (90 µm -106 µm)

3. Results

3.1. Microstructural characterization

Fig. 6 shows the cross sections of the different grain fractions of the SFTC particle reinforced NAB matrix directly after LMI. As seen in Fig. 6, SFTC particles were distributed all over the width and depth of the melt pool. The selected samples represent the best outcomes obtained from the experiments. Due to a higher density of SFTC particles, experiments have demonstrated the presence of a hard particle-free zone for larger particle sizes. The powder flow rate had to be increased

with increasing particle sizes to eliminate a hard particle-free zone. It is explained by (Ramoliya et al. 2023) how to compute the homogeneity of the layer. According to it, the distribution of particles in the layer is homogeneous. The particle content using SFTC in the NAB matrix lies between 20% - 40%.

As a second reinforcing material, niobium carbide has been used. A cross-section of the micrographs is shown in Fig. 7. An MMC layer without any cracks and pores can be produced. In contrast to SFTC particles, NbC particles required a lower powder flow rate to form an MMC layer. This is due to NbC's density being around half that of SFTC. To improve particle distribution in the melt pool, laser power is increased proportionally to particle size. Just like SFTCs, the layer's homogeneity is proven. The NAB matrix has a homogenous distribution of NbC particles, as can be deduced. The particle content of the NAB matrix containing NbC ranges between 20% and 30%.

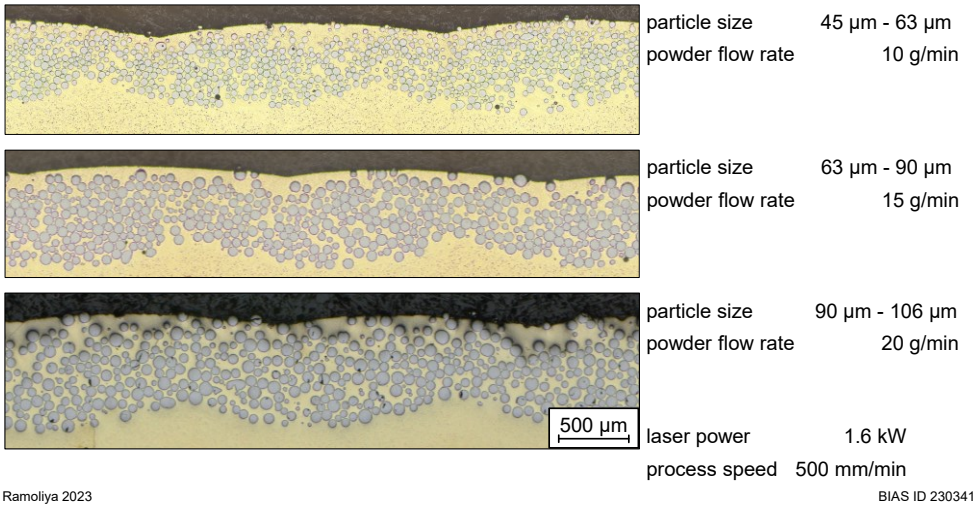

Fig. 6. Metallographic image obtained from SFTC-reinforced NAB substrate with different particle sizes and different powder flow rates.

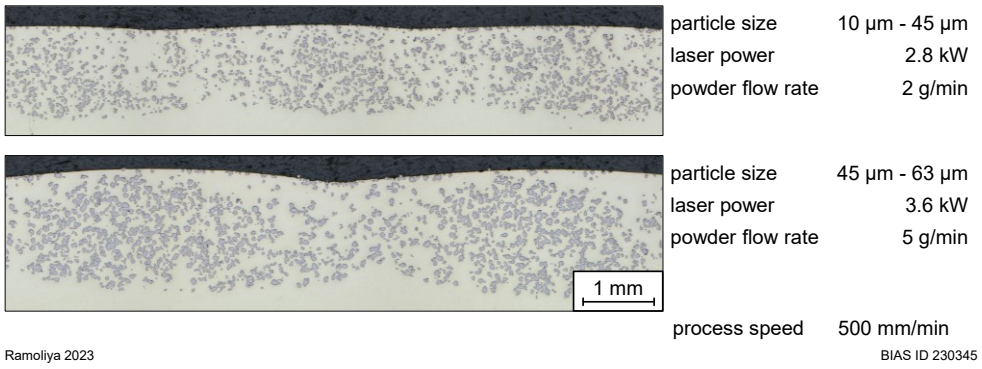

Fig. 7. Metallographic image obtained from NbC reinforced NAB substrate with different particle sizes and different powder flow rates.

3.2. Cavitation erosion behaviour

Fig. 8 shows the cumulative mass loss of unpolished NbC reinforced samples over time, as well as a reference sample (NAB). The reinforced samples show a higher mass loss rate in the initial periods, which is 3 to 4 times higher compared to reference samples, and ended up with 33% more mass loss compared to a reference sample after 140 hr of CE test. The mass loss rate of both NbC particle-based samples is identical.

The roughness of respective polished reinforced samples is listed in Table 3. The arithmetical mean height (Sa) for all reinforced samples was < 0.2 µm, while the maximum heights (Sz) for NAB + NbC (45 µm - 63 µm) and NAB + SFTC

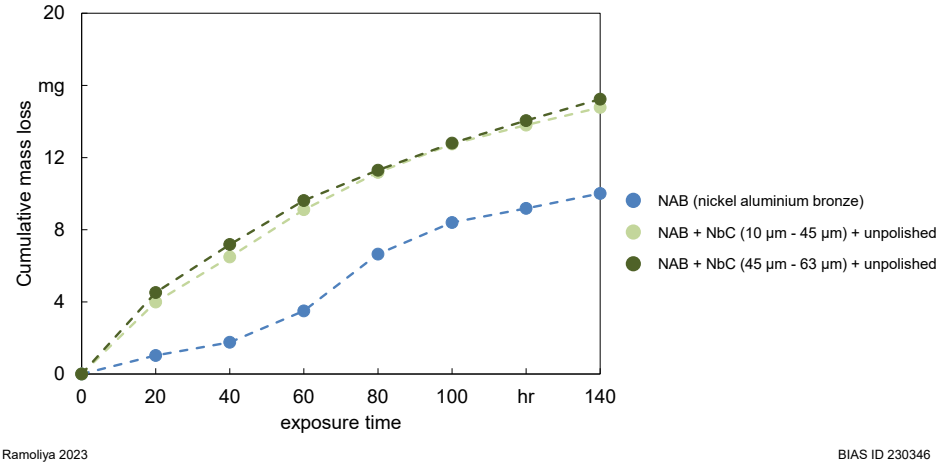

Fig. 8. Cumulative mass loss as a function of time for unpolished NbC reinforced and NAB alloy for 140 hr of CE test.

(45 µm - 63 µm) reinforced samples were 2.431 µm and 3.663 µm respectively. The maximum height of the remaining samples was less than 2 µm.

Table 3. Average (Sa) and maximum (Sz) roughness values for all prepared samples.

samples	Arithmetical mean height Sa (µm)	Maximum height Sz (µm)
NAB + NbC (10 µm - 45 µm)	0.087	1.424
NAB + NbC (45 µm - 63 µm)	0.095	2.431
NAB + SFTC (45 µm - 63 µm)	0.125	3.663
NAB + SFTC (63 µm - 90 µm)	0.197	1.999
NAB + SFTC (90 µm - 106 µm)	0.18	1.331

The average percentage of erosion of particles and surfaces of the SFTC-reinforced sample is shown in Table 4. According to the data presented in Table 4, the density of NAB + SFTC (45 µm – 63 µm), NAB + SFTC (63 µm - 90 µm), and NAB + SFTC (90 µm - 106 µm) is 13.36 g/cm^3, 12.45 g/cm^3, and 12.64 g/cm^3 respectively. In the following section, these density data will be utilized to determine volume loss.

Table 4. The average percentage of erosion of particles and surfaces of all SFTC-reinforced cavitation samples.

Samples	Percentage of erosion of particle	Percentage of erosion of surface
NAB + SFTC (45 µm - 63 µm)	72%	28%
NAB + SFTC (63 µm - 90 µm)	60.65%	39.35%
NAB + SFTC (90 µm -106 µm)	63%	37%

The cumulative volume loss (CVL) of the investigated samples as a function of exposure time is shown in Fig. 9. The cumulative volume loss of NAB (nickel aluminium bronze) is 1.37 mm^3 after 140 hours of CE testing. After 40 hours, the volume loss rate of NAB increased, then ended up being stable after 100 hours. NAB + NbC (10 µm - 45 µm) experienced the lowest cumulative volume loss 0.43 mm^3 during the CE test, while CVL for NAB + NbC (45 µm – 63 µm) 0.80 mm^3, which is half of NAB's. During the CE test, the volume loss rate of both NbC-reinforced samples remains constant.

Initially, NAB + SFTC (90 µm - 106 µm) exhibited a greater volume loss rate than the other two samples and ended at 2.2 mm^3. Whereas NAB + SFTC (45 µm - 63 µm) experienced an excessive cumulative volume loss of 2.3 mm^3 in the given environment after 140 hours of CE testing, which is the highest amongst the investigated samples and ca. 5 times and 2 times higher than NAB + NbC (10 µm - 45 µm) and NAB reference samples, respectively.

The mean depth of erosion (MDE) and the mean depth of erosion rate (MDER) were determined using Eqs. 1 and 2 after the testing period i.e. 140 hr. The SFTC-reinforced samples had the greatest MDER (0.55 µm/hr) of any sample, while the NbC-reinforced samples had the lowest (0.1 µm/hr). A material's resistance to CE damage can be determined by normalised CE resistance as per Eqs. 3 [19]. The calculated normalised CE resistance is shown in Fig. 10. The normalised cavitation erosion resistance of the NAB substrate is 2.89 hr/µm. According to Fig. 10, NAB+NbC (10 µm - 45 µm) shows the

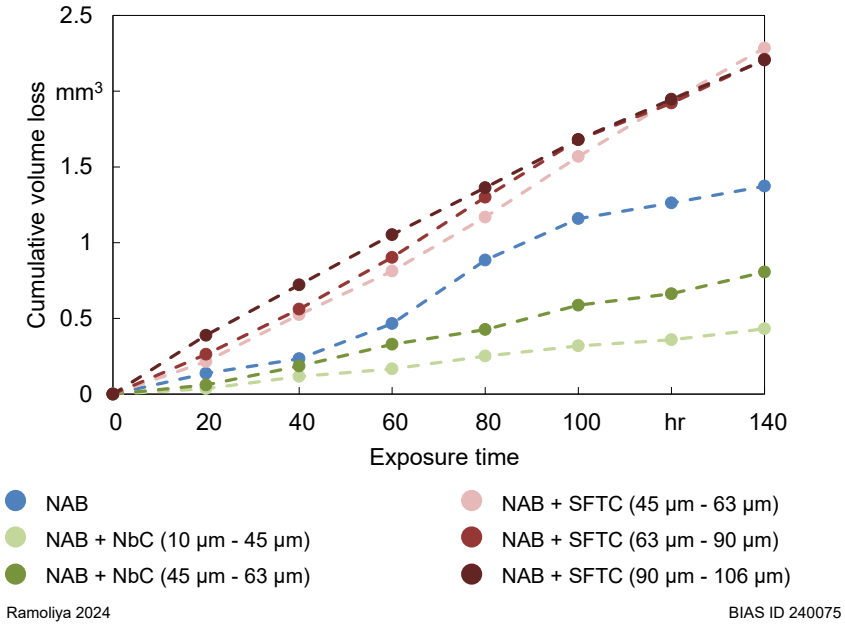

Fig. 9. Cumulative volume loss as a function of time for polished SFTC reinforced, NbC reinforced, and NAB alloy for 140 hr of CE test.

highest resistance to CE, which is approx. 2 times greater than NAB+NbC (45 µm - 63 µm) and 4 times greater than NAB. Comparing all the SFTC particle samples to the NAB substrate, the resistance against CE is lower, while NAB+NbC (10 µm - 45 µm) shows 5 times greater resistance to CE concerning all SFTC-reinforced samples.

The topology of the end faces of all samples after 140 hr are shown in Fig. 11. The NAB sample's eroded surface is covered by many pits and crates as demonstrated in Fig. 11 (a). It has also been noted that CE originates from the edges of the NAB sample (See Fig. 11 (a)). The CE for the NbC-reinforced materials emanate from the edge, as illustrated in Fig. 11 (b & c). In contrast, as Fig. 11 (d, e, & f) depicts, CE for SFTC-reinforced samples originates from the center of the samples. Fig. 11 (d, e, f) demonstrates that, following the same cavitation erosion period, the surface of the SFTC-reinforced samples is more severely damaged, with a higher surface damage area than the NAB and NbC reinforced samples. The damaged surface of the SFTC samples were covered in pits and cavities, which finally led to fissures. On the other hand, the NAB+NbC (10 µm - 45 µm) sample has the smallest damaged depth and smoothest damaged surface, resulting in the highest CE resistance.

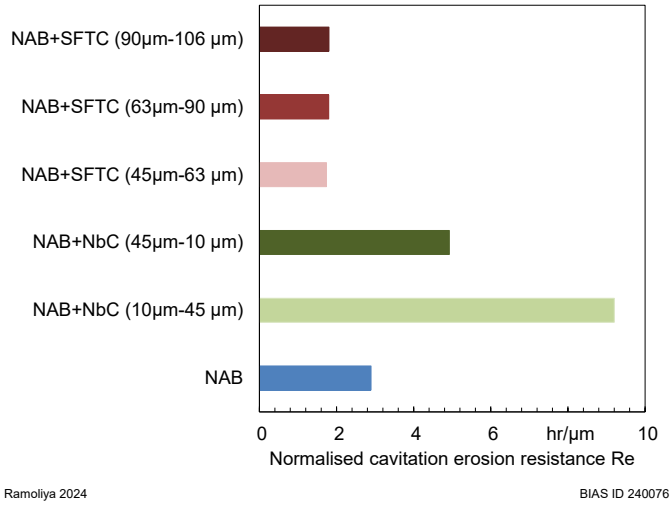

Fig. 10. Normalised CE resistance of various samples.

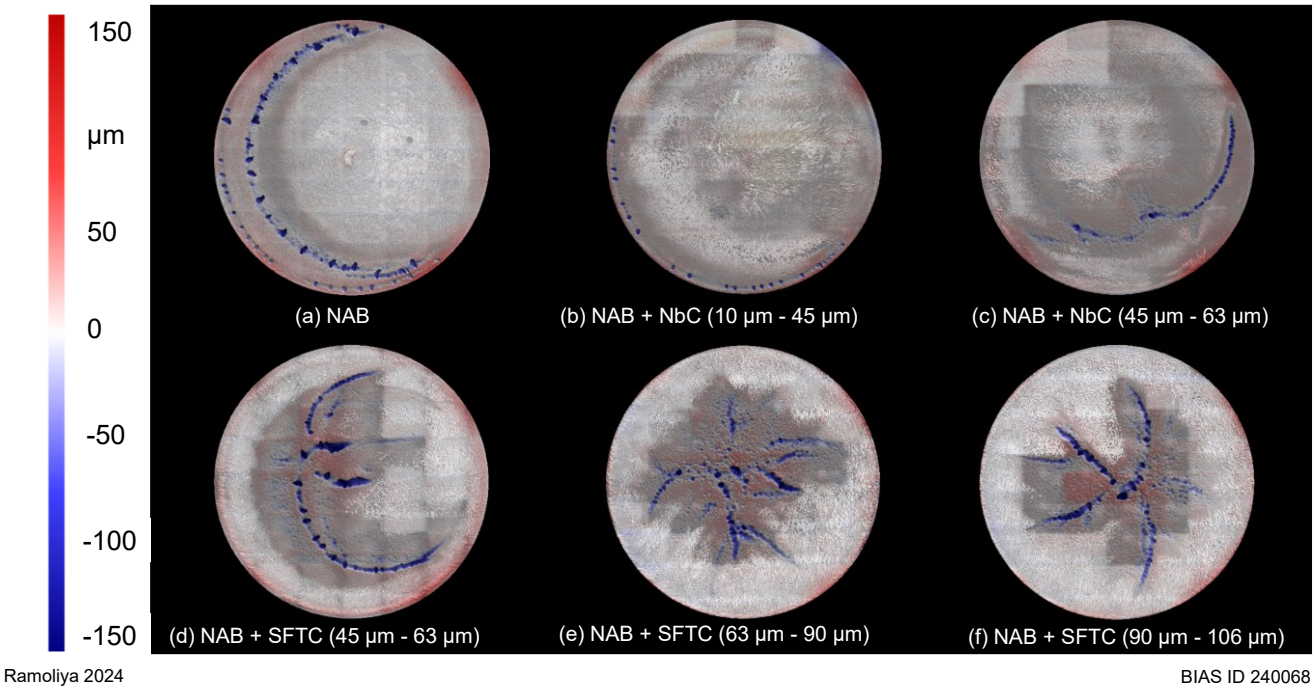

Fig. 11. Topology of end faces of (a) NAB, (b) small NbC reinforced, (c) large NbC reinforced, (d) small SFTC reinforced, (e) intermediate SFTC reinforced, and (f)larger SFTC reinforced MMC sample after 140 hr of CE test.

4. Discussion

NbC dispersion is a potential way to lower the cavitation erosion (CE) losses in the aluminum bronze alloy, as the primary evidence indicates that it performed best under the tested conditions, followed by SFTC coating (Ramoliya et al. 2025).

According to Fig. 8, the unpolished reinforced samples show a higher mass loss compared to NAB samples. It could be because of the higher surface roughness of the samples. A higher surface roughness level increases the density of bubble nucleation near the surface of the reinforced sample, which causes more impact of the collapsing bubble on the surface and

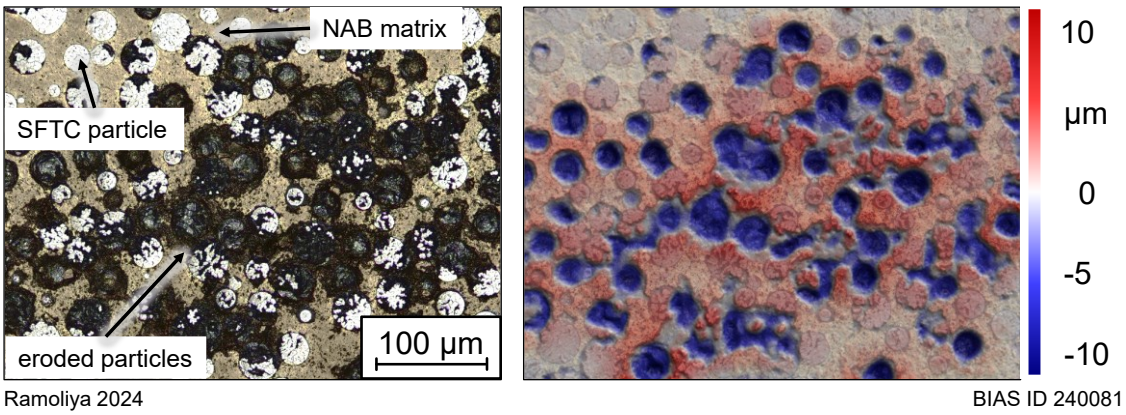

Fig. 12. Optical (left) and 3D-scan images of SFTC-reinforced sample after 2.5 hr of CE test.

results from this more mass loss of the coating. This may suggest that the initial surface roughness plays a great role in the cavitation erosion damage of the coatings. The similar results were reported by (Lin et al. 2017; Espallargas et al. 2008).

Considering the MMC samples in this investigation as a dual-phase system consisting of (i) the matrix phase, which was a solid solution NAB with carbides scattered in it, and (ii) the ceramic phase, which was the SFTC and NbC that remained in the melt layer. In a dual-phase system, the major CE resistance is determined by the resistance of the weaker phase, which is eroded preferentially. Microcracks are initiated easily at the edge of pre-existing pits under CE impulses. With the progress of CE, these microcracks grew, coalesced, and propagated along with the pre-existing defects or interfaces between splats, forming small and shallow pits on the coating surface. The cracks in each direction are interconnected to each other, causing lamellar spalling of the coatings. Simultaneously, a multitude of pits and cracks is detected in the bottom of the craters, allowing additional sources for CE to spall material (See Fig. 11).

As shown in Fig.11, CE for SFTC-reinforced samples originate from the center of the samples. The CE for SFTC reinforced samples may start from the crack formation on the SFTC particle surface shown in Fig. 12 taken 2.5 hr after the CE test. Fig. 12 suggests that brittle fracture of SFTC particles under cavitation assault is the first cause of cavitation damage. The SFTC particles in each sample reacted to the cavitation assault in the same manner. Lo et al. observed that the erosion of SFTC-reinforced MMC layers appeared to be initiated by defects on the SFTC surface, concerning the cavitation behavior of these layers (Lo et al. 2003).

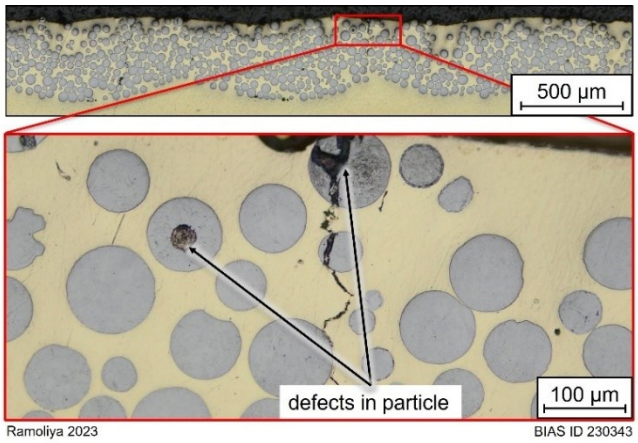

Fig. 13. Cross-section of the SFTC coatings.

The presence of SFTC defects in the MMC layers (pores and fractures shown in Fig. 13) and the lack of fractures in the original SFTC particles indicate that these defects were caused by direct laser irradiation and were not intrinsic to the SFTC particles as received. However, the MMC samples' matrix encountered ductile fracture during the CE test. The interfacial region between the SFTC particles and the matrix was not a weak location for any of the SFTC-reinforced MMC samples that were investigated, as cavitation damage did not appear to be initiated there (as shown in Fig. 12). As seen in Fig. 11 (d-f), the coatings layer exhibits many cavities. These cavities are the result of a localized stress concentration generated by the microjets' extreme pressure.

In contrast to SFTC, NbC does not fracture, and it also avoids crater formation. NbC particles do not exhibit any undesirable deformation during LMI, which results in excellent hardness and enhances the coating's resistance to wear (Wank et al. 2023; Yufan et al. 2020). Ahmed et al. claim the cavitation wear rate was determined by the combination of hardness and fracture toughness, as fracture dominated the cavitation erosion (Singh et al. 2022; A. Algoburi, R. Ahmed, V. Kumar 2024).

In the present study, it was observed that the microhardness of NbC is higher than that of NAB alloy. Because the hard phase of NbC coatings is more prevalent and well-integrated with the matrix, NbC particles are more difficult to remove during the CE process, giving NbC coatings an increased hardness. As shown in Fig. 14, the base matrix erodes first in the CE of a NbC reinforced sample, whereas the erosion of NbC particles is less severe. Hence, it can be said that the CE for NbC moves through the base matrix to the NbC particles. The CE of NbC coatings also originate from boundaries like the CE of the NAB sample. The eroded surface of NbC coatings is covered by pits and crates as shown in Fig. 11 (b, c). Beyond its

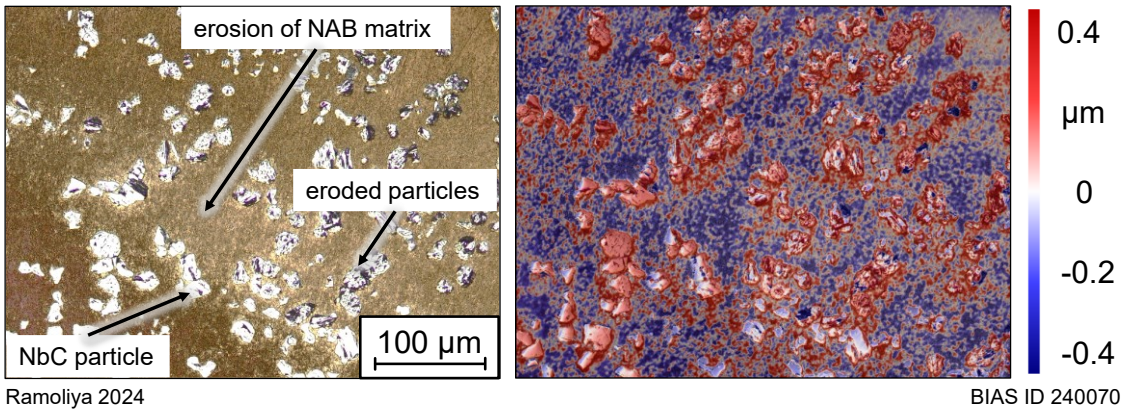

Fig. 14. Optical (left) and 3D-scan images of NbC-reinforced sample after 2.5 hr of CE test.

mechanical properties, the structure of the material also affects CER. In summary, for NAB+NbC (10 µm - 45 µm) and NAB+NbC (45 µm - 63 µm) reinforced samples, service life increased by a factor of 3 and 2 compared to the NAB sample. Bregliozzi claims that there is a connection between CER and grain size and good CER is ensured by small grain sizes when applying coatings (Bregliozzi et al. 2005). The results show that small NbC-reinforced samples provided twice as much CER as large NbC-reinforced samples. The reason for this is that the coatings become more resilient to deformation when the small particles interact with the matrix. Hence, it is recommended to use the small particle size for higher resistance against CE.

5. Conclusion

Using the laser melt injection (LMI) method, MMC layers are made of SFTC and NbC hard particles in an NAB matrix. It has been possible to create MMC layers with homogeneous particle distribution. A study was conducted on cavitation erosion (CE) behavior at 25°C in deionised water. The conclusions that follow are obtained.

- Cavitation wear resistance was determined by the material's initial roughness, hardness, and fracture toughness.
- After a 140-hour CE test, NbC hard particles have been shown to lower the CE losses in NAB alloy by a factor 3. For greater cavitation erosion resistance (CER), it is advised to use a small niobium carbide particle (10µm<p<45µm).
- Compared to NAB alloy, SFTC-reinforced samples eroded more quickly. The lower fracture toughness and defects of the SFTC particles, which commence the CE, were found to be the main mechanisms of failure. The indications of CE in the coatings are discovered to be the development of bigger craters, cavities, and splat debonding.
- The optimal combination of microhardness and fracture toughness of NbC may be responsible for its extraordinary CER, which delays the beginning and development of cavitation erosion.

Acknowledgements

The ZIM-project no. KK5274702AG1 was funded by the Federal Ministry for Economic Affairs and Energy (BMWi) via the German Federation of Industrial Research Associations (AiF) in accordance with the policy to support the Central Innovations of Medium-Sized Enterprises (ZIM) based on a decision by the German Bundestag.

References

A. Algoburi, R. Ahmed, V. Kumar (Hg.) (2024): Cavitation Erosion in HVOF Thermally Sprayed WC-NiCrBSi Coatings. International Thermal Spray Conference and Exhibition ITSC 2024. Milan/Italy, April 29 - May 1. Heriot-Watt University, School of Engineering and Physical Sciences, Edinburgh EH14 4AS, UK. 393 Bände: DVS-Berichte.

Bregliozzi, G.; Di Schino, A.; Ahmed, S.I.-U.; Kenny, J. M.; Haefke, H. (2005): Cavitation wear behaviour of austenitic stainless steels with different grain sizes. In: *Wear* 258 (1-4), S. 503–510. DOI: 10.1016/j.wear.2004.03.024.

Espallargas, N.; Berget, J.; Guilemany, J. M.; Benedetti, A. V.; Suegama, P. H. (2008): Cr3C2–NiCr and WC–Ni thermal spray coatings as alternatives to hard chromium for erosion–corrosion resistance. In: *Surface and Coatings Technology* 202 (8), S. 1405–1417. DOI: 10.1016/j.surfcoat.2007.06.048.

Freiße, H.; Bohlen, A.; Seefeld, T. (2019): Determination of the particle content in laser melt injected tracks. In: *Journal of Materials Processing Technology* 267, S. 177–185. DOI: 10.1016/j.jmatprotec.2018.12.018.

García-García, D. M.; García-Antón, J.; Igual-Muñoz, A.; Blasco-Tamarit, E. (2006): Effect of cavitation on the corrosion behaviour of welded and non-welded duplex stainless steel in aqueous LiBr solutions. In: *Corrosion Science* 48 (9), S. 2380–2405. DOI: 10.1016/j.corsci.2005.09.009.

GTV Verschleißschutz GmbH: Material Product Data Sheet Niobium Carbide Powder for Laser Cladding.

Gualtieri, T.; Bandyopadhyay, A. (2017): Niobium carbide compostie coatings on SS304 using laser engineered net shaping (LENS™). In: *Materials Letters* 189, S. 89–92. DOI: 10.1016/j.matlet.2016.11.071.

Kolbe G (2005): Beitrag zur Erhöhung der Verschleißbeständigkeit von Bauteilen aus TiAl6V4 durch Dispergieren/Legieren mit Diboriden. Dissertation. Fakultät für Maschinenbau der Technischen Universität Chemnitz, Chemnitz. Online verfügbar unter https://monarch.qucosa.de/id/qucosa:18284.

Kwok, C. T.; Man, H. C.; Cheng, F. T.; Lo, K. H. (2016): Developments in laser-based surface engineering processes: with particular reference to protection against cavitation erosion. In: *Surface and Coatings Technology* 291, S. 189–204. DOI: 10.1016/j.surfcoat.2016.02.019.

Li, Zhiyuan; Yan, Hua; Zhang, Peilei; Guo, Jialong; Yu, Zhishui; Ringsberg, Jonas W. (2021): Improving surface resistance to wear and corrosion of nickel-aluminum bronze by laser-clad TaC/Co-based alloy composite coatings. In: *Surface and Coatings Technology* 405, S. 126592. DOI: 10.1016/j.surfcoat.2020.126592.

Lin, Jinran; Wang, Zehua; Cheng, Jiangbo; Kang, Min; Fu, Xiuqing; Hong, Sheng (2017): Effect of Initial Surface Roughness on Cavitation Erosion Resistance of Arc-Sprayed Fe-Based Amorphous/Nanocrystalline Coatings. In: *Coatings* 7 (11), S. 200. DOI: 10.3390/coatings7110200.

Lo, K. H.; Cheng, F. T.; Man, H. C. (2003): Cavitation erosion mechanism of S31600 stainless steel laser surface-modified with unclad WC. In: *Materials Science and Engineering: A* 357 (1-2), S. 168–180. DOI: 10.1016/S0921-5093(03)00216-8.

Oerlikon Metco: Material Product Data Sheet Spherical Cast Tungsten Carbide Powder for Laser Cladding.

Peters, Andreas; Lantermann, Udo; el Moctar, Ould (2018): Numerical prediction of cavitation erosion on a ship propeller in model- and full-scale. In: *Wear* 408-409, S. 1–12. DOI: 10.1016/j.wear.2018.04.012.

Ramoliya, M.; Bohlen, A.; Seefeld, T. (Hg.) (2025): Laser melt injection of niobium carbide on aluminium bronze substrates for enhanced cavitation erosion resistance. NOLAMP. Copenhagen. In Print.

Ramoliya, M.; Bohlen A; Seefeld T (Hg.) (2023): Distribution of SFTC, NbC, and Cr3C2 particles in aluminium bronze by laser melt injection. Laser in Manufacturing (LiM). Munich/Germany: Proc. of Lasers in Manufacturing Conference 2023 (LiM 2023). German Scientific Laser Society/Wissenschaftliche Gesellschaft Lasertechnik e.V. (WLT e.V.).

Singh, Navneet K.; Vinay, Gidla; Ang, Andrew S.M.; Mahajan, Dhiraj K.; Singh, Harpreet (2022): Cavitation erosion mechanisms of HVOF-sprayed Ni-based cermet coatings in 3.5% NaCl environment. In: *Surface and Coatings Technology* 434, S. 128194. DOI: 10.1016/j.surfcoat.2022.128194.

Song, Qi-Ning; Xu, Nan; Bao, Ye-Feng; Jiang, Yong-Feng; Gu, Wei; Zheng, Yu-Gui; Qiao, Yan-Xin (2017): Corrosion and Cavitation Erosion Behaviors of Two Marine Propeller Materials in Clean and Sulfide-Polluted 3.5% NaCl Solutions. In: *Acta Metall. Sin. (Engl. Lett.)* 30 (8), S. 712–720. DOI: 10.1007/s40195-017-0602-7.

Standard test method for cavitation erosion using vibratory apparatus, G32-16, Annual Book of ASTM (2016). West Conshohocken, PA.

Tang, C. H.; Cheng, F. T.; Man, H. C. (2006): Laser surface alloying of a marine propeller bronze using aluminium powder. In: *Surface and Coatings Technology* 200 (8), S. 2602–2609. DOI: 10.1016/j.surfcoat.2004.12.021.

Tang, C.H; Cheng, F.T; Man, H.C (2004): Improvement in cavitation erosion resistance of a copper-based propeller alloy by laser surface melting. In: *Surface and Coatings Technology* 182 (2-3), S. 300–307. DOI: 10.1016/j.surfcoat.2003.08.048.

V. Ocelík; S. Nijman; R. van Ingen; U. Oliveira; J.Th.M. De Hosson (2003): Laser Melt Injection Of Hard Ceramic Particles Into Al And Ti Alloys† Processing, Microstructure And Mechanical Behaviour. In: *WIT Transactions on Engineering Sciences* 39. DOI: 10.2495/SURF030141.

Wank, Andreas; Schmengler, Christian; Krause, Annika; Müller-Roden, Karin; Wessler, Tobias (2023): Environmentally Friendly Protective Coatings for Brake Disks. In: *J Therm Spray Tech* 32 (2-3), S. 443–455. DOI: 10.1007/s11666-022-01459-0.

Yufan, S.; Hanguang, F.; Xuelong, P.; Shuting, S.; Jian, L.; Yongping, L. (2020): Effect of process parameters and niobium carbide addition on microstructure and wear resistance of laser cladding nickel‐based alloy coatings. In: *Materialwissenschaft Werkst* 51 (1), S. 54–65. DOI: 10.1002/mawe.201800221.

Zhao, Nana; Xu, Yunhua; Huang, Xing; Zhong, Lisheng; Lu, Jiuli (2016): Microstructure and wear properties of niobium carbide particulates gradient-distribution composite layer fabricated in situ. In: *Ceramics International* 42 (16), S. 18507–18515. DOI: 10.1016/j.ceramint.2016.08.188.

Zheng, Y. G.; Luo, S. Z.; Ke, W. (2008): Cavitation erosion–corrosion behaviour of CrMnB stainless overlay and 0Cr13Ni5Mo stainless steel in 0.5M NaCl and 0.5M HCL solutions. In: *Tribology International* 41 (12), S. 1181–1189. DOI: 10.1016/j.triboint.2008.02.011.